NASA/TM—1998-208814

Comparison of Computational–Model and Experimental–Example Trained Neural Networks for Processing Speckled Fringe Patterns

A.J. Decker, E.B. Fite, S.A. Thorp, and O. Mehmed
Lewis Research Center, Cleveland, Ohio

November 1998

The NASA STI Program Office . . . in Profile

Since its founding, NASA has been dedicated to the advancement of aeronautics and space science. The NASA Scientific and Technical Information (STI) Program Office plays a key part in helping NASA maintain this important role.

The NASA STI Program Office is operated by Langley Research Center, the Lead Center for NASA's scientific and technical information. The NASA STI Program Office provides access to the NASA STI Database, the largest collection of aeronautical and space science STI in the world. The Program Office is also NASA's institutional mechanism for disseminating the results of its research and development activities. These results are published by NASA in the NASA STI Report Series, which includes the following report types:

- TECHNICAL PUBLICATION. Reports of completed research or a major significant phase of research that present the results of NASA programs and include extensive data or theoretical analysis. Includes compilations of significant scientific and technical data and information deemed to be of continuing reference value. NASA's counterpart of peer-reviewed formal professional papers but has less stringent limitations on manuscript length and extent of graphic presentations.

- TECHNICAL MEMORANDUM. Scientific and technical findings that are preliminary or of specialized interest, e.g., quick release reports, working papers, and bibliographies that contain minimal annotation. Does not contain extensive analysis.

- CONTRACTOR REPORT. Scientific and technical findings by NASA-sponsored contractors and grantees.

- CONFERENCE PUBLICATION. Collected papers from scientific and technical conferences, symposia, seminars, or other meetings sponsored or cosponsored by NASA.

- SPECIAL PUBLICATION. Scientific, technical, or historical information from NASA programs, projects, and missions, often concerned with subjects having substantial public interest.

- TECHNICAL TRANSLATION. English-language translations of foreign scientific and technical material pertinent to NASA's mission.

Specialized services that complement the STI Program Office's diverse offerings include creating custom thesauri, building customized data bases, organizing and publishing research results . . . even providing videos.

For more information about the NASA STI Program Office, see the following:

- Access the NASA STI Program Home Page at ***http://www.sti.nasa.gov***

- E-mail your question via the Internet to help@sti.nasa.gov

- Fax your question to the NASA Access Help Desk at (301) 621-0134

- Telephone the NASA Access Help Desk at (301) 621-0390

- Write to:
  NASA Access Help Desk
  NASA Center for AeroSpace Information
  7121 Standard Drive
  Hanover, MD 21076

NASA/TM—1998-208814

Comparison of Computational–Model and Experimental–Example Trained Neural Networks for Processing Speckled Fringe Patterns

A.J. Decker, E.B. Fite, S.A. Thorp, and O. Mehmed
Lewis Research Center, Cleveland, Ohio

Prepared for the International Conference on Optical Technology and Image Processing in Fluid, Thermal and Combustion Flow cosponsored by the Visualization Society of Japan and SPIE - The International Society of Optical Engineering Yokohama, Japan, December 7–9, 1998

National Aeronautics and Space Administration

Lewis Research Center

November 1998

Available from

NASA Center for Aerospace Information
7121 Standard Drive
Hanover, MD 21076
Price Code: A03

National Technical Information Service
5285 Port Royal Road
Springfield, VA 22100
Price Code: A03

Proceedings of VSJ-SPIE98
December 6—9, 1998, Yokohama, Japan
AB002

Comparison of Computational-Model and Experimental-Example Trained Neural Networks for Processing Speckled Fringe Patterns

Decker, A. J., Fite, E. B., Thorp, S. A., Mehmed, O.

NASA Lewis Research Center
Cleveland, Ohio 44135
USA
adecker@lerc.nasa.gov

Abstract: The responses of artificial neural networks to experimental and model-generated inputs are compared for detection of damage in twisted fan blades using electronic holography. The training-set inputs, for this work, are experimentally generated characteristic patterns of the vibrating blades. The outputs are damage-flag indicators or second derivatives of the sensitivity-vector–projected displacement vectors from a finite element model. Artificial neural networks have been trained in the past with computational-model-generated training sets. This approach avoids the difficult inverse calculations traditionally used to compare interference fringes with the models. But the high modeling standards are hard to achieve, even with fan-blade finite-element models.

Keywords: Neural Networks, Interferometry, Electronic Holography, Image Processing, Speckle Metrology

1. Introduction

There is a continuing need to convert whole-field data such as interference patterns of flows and structures into two and three-dimensional distributions of properties. The traditional viewpoint is that the instrument system should convert the raw optical pattern to a two or three-dimensional distribution of the quantity of interest such as velocity, density, displacement or strain. The instrument-derived results are then compared ostensibly with predictions of computational models or are used directly to operate test facilities. That viewpoint no doubt is most friendly to the users of optical measurement instrumentation, but suffers from some serious practical and scientific defects. The conversion of interference patterns into densities of flows or strain fields of structures, for example, is generally ill posed and requires often-arbitrary regularization procedures. The measurement process invariably contains some untested assumptions: one classical example is the assumption in laser anemometry or particle image velocimetry that seed particles track flows. A working instrument may not be well matched to the environmental conditions or operating conditions required by a user. Finally, a whole-field optical measurement system may not have the processing speed to meet real-time requirements.

An alternative viewpoint of whole-field data conversion has been under test at NASA Lewis Research Center for a number of years. The concept is to compute an optical pattern by combining a phenomenological model of a flow or structure with a model of the optical measurement process. Measured patterns are then compared with the computed patterns to identify a best match between the measured and model-generated flow or structural conditions, or whether a match even exists. This approach avoids ill-posed inverse calculations. The ultimate user or customer provides the phenomenological models and is directly involved in determining whether the instrument will meet customer requirements. This approach can be added to existing optical measurement systems, but it requires a fast interface between the computational-model-generated patterns and the measured patterns.

Artificial neural networks, particularly the feedforward neural network, are being tested at Lewis as fast interfaces between computational-model-generated fringe patterns and measured fringe patterns. Our initial application of the neural network interface was to computed tomography (Decker, 1993). Neural networks have been used during the past two years to process the time-average characteristic patterns computed from electronic holograms of vibrating structures. Neural-net processing of these holograms constitutes a complete test of the concept of using a neural-net interface for flows or structures. Finite element models of vibrating fan blades are the phenomenological models. An optical model of electronic holography, complete with techniques for handling the laser speckle effect, has been developed (Decker et al., July 1997). There is a strong customer interest in the technique and a willingness to participate in developing the neural net interface since there is a need to display strain or damage information for fan blades. Finally, neural net processing of characteristic patterns has been demonstrated at up to 30 frames per second (Decker et al., May 1998), thereby providing a fast interface.

The following question has surfaced during this work with neural-net interfaces: Do the finite element models normally used to design fan blades generate sufficiently accurate patterns to train the neural networks? A major reason for testing the neural net concept with structural models was the assumption that structural models would be better known than flow models. As mentioned in the references above, the assumption proved correct for cantilever plates. But recent work with twisted blades has indicated that normal design models may not provide enough accurate detail to train the

neural-net interface, particularly at the resolutions required for damage detection. Neural nets have proven to be very exacting for comparing model generated patterns with measured patterns.

This paper is a comparison of neural-net processing of experimental-example with model-generated characteristic patterns of twisted fan blades. The blades were constructed specifically for these tests, but have vibration properties similar to the properties of blades in bladed disks (blisks). Three blades were constructed, and one blade was intentionally cracked through shaker-induced high-cycle fatigue failure. The characteristic patterns were generated using two-frame electronic time-average holography, where the phase of the reference beam was shifted by 180 degrees between alternate frames. Subtraction of the frames then yielded high-contrast characteristic patterns.

2. Neural-Net Training Records

The architecture of the artificial neural networks and the composition of the training records have been discussed in detail previously (Decker et al., July 1997), (Decker et al., May 1998). The computer platforms, neural net software and video were also discussed. Both publications treated cantilever plates as examples; whereas this paper treats a twisted blade as an example. The previous publications discussed model-trained artificial neural networks exclusively; whereas this paper discusses both model and experimental-example trained neural nets. The following discussion reviews the neural nets and training records briefly and introduces some new features.

Software created at NASA Lewis Research Center is used to generate the training records and training sets automatically. This software, together with the package used to create the feedforward neural networks and the video used to record the holograms, are resident in a SGI O2 workstation. The combination has been demonstrated at up to 30 frames per second for neural-net processing of characteristic patterns.

The training sets relevant to this paper contain a few hundred training records. Each training record contains an input vector and an output vector. The inputs are normalized in the range 0 to 1 , and the outputs are normalized between 0.2 and 0.8 for the sigmoid (logistic) transfer functions of the neural networks. Other neural-net architectures have been trained. But the compactness and noise handling ability of the feedforward net makes it definitely superior for processing the speckled characteristic patterns from time-average holography.

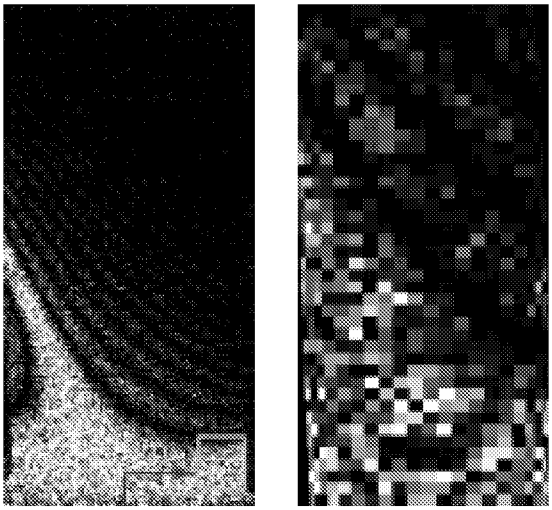

Fig. 1. Characteristic or time-average patterns of first mode of twisted blade: (a) at CCD-camera resolution, where the insert shows the region measured for crack detection, (b) at finite-element resolution.

The input vectors always are finite-element-resolution characteristic fringe patterns with the scan lines packed in order. The design-grade finite element models and workstations used to design compressor blades handle a maximum of about 5000 elements. Hence, the input vectors will contain a few hundred to a few thousand pixel values. Figure 1 shows both CCD and finite-element resolution characteristic patterns (not at the same vibration amplitude) for the first bending mode of the twisted blade used as an example in this paper. The pixel sizes in the finite-element-resolution pattern were calculated from the design model described in the next section. The input vector might contain a full-blade pattern or a pattern from a magnified small region of the blade. The insert in the CCD resolution pattern in fig. 1 was zoomed and measured for crack detection, for example. The CCD cameras are always 640x480 pixel NTSC cameras.

As reported previously (Decker et al., July 1997), the neural networks can be taught to ignore the laser speckle effect. To accomplish this objective, independent speckle patterns, equal in number to about 10 percent of the number of linearly independent input vectors, must be presented during training. Hence, a training set composed of 1000-pixel inputs would need approximately 100 linearly independent speckle patterns per characteristic pattern. Experimentally, sampling

at random locations within the large pixels of the finite-element-resolution array is used to generate the independent speckle patterns. This step is necessary since the speckle patterns remain highly correlated from frame to frame on the vibration isolation table used to conduct the experiments. Theoretically, a random number generator is used to create linearly independent speckle patterns from the models (discussed in the next section). Sampling grids and pixel sizes are determined from the finite element models and are generally not uniform. Figure 2 plots the sampling locations on the twisted blades discussed in this paper.

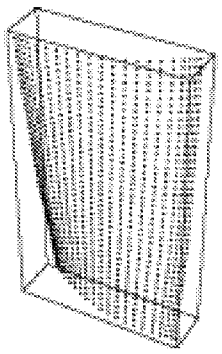

Fig. 2. Finite-element-resolution sampling grid for twisted blades.

The output vectors are either model generated patterns or damage flags. Finite-element-model-generated strain patterns can be used as the output. But the second spatial derivatives of the sensitivity-vector-projected displacement-amplitude vectors of the vibrating object are more appropriate for electronic holography. This claim can be understood by noting that the visualized characteristic pattern is proportional to

$$\text{(Speckle Pattern)} \times J_0(2\pi \mathbf{K} \cdot \boldsymbol{\delta})$$

where $\mathbf{K}$ is the holographic sensitivity vector (Vest, 1979) and $\boldsymbol{\delta}$ is the displacement-amplitude vector. The second derivatives of $\mathbf{K} \cdot \boldsymbol{\delta}$ were discovered to provide sensitive detection of blade cracking. Interestingly the bending induced strain of a plate can be computed from the second derivatives of the normal components of $\boldsymbol{\delta}$ in a local coordinate system. But holography visualizes a projection of $\boldsymbol{\delta}$ on $\mathbf{K}$ rather than the normal. The displacement distributions are obtained from the finite element model. Figure 3 shows chord-wise second derivatives of the sensitivity-vector-projected displacements from the insert in fig. 1. Model predicted patterns are shown for cracked and undamaged twisted blades.

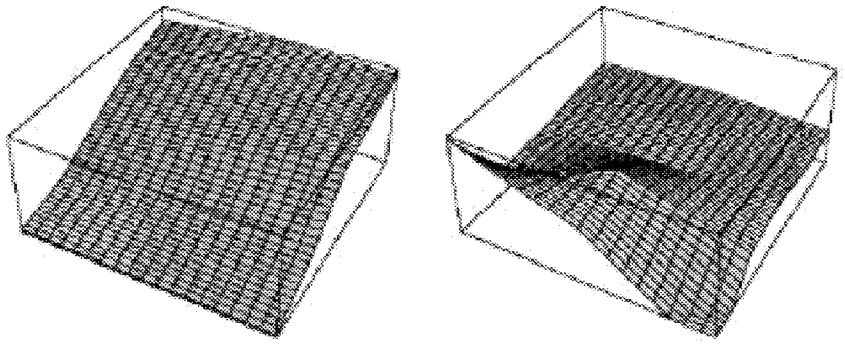

(a) (b)

Fig. 3. Model-predicted chord-wise second derivative of $\mathbf{K} \cdot \boldsymbol{\delta}$ of fig. 1: (a) for undamaged blade, (b) for cracked blade.

These plots are slightly distorted by being plotted on a uniform grid. The output vector of the training record will then contain a few hundred to a few thousand components. Sometimes, a simple indication or flag whether a blade is damaged or undamaged is adequate. The output of the net, for example, can be a three-component vector. One component indicates a cracked blade; one component indicates an undamaged blade; and one component indicates that the pattern is not known. We display this information by coloring the fringe patterns red, green and yellow, respectively. The damage flag can be used with model generated or experimental samples.

The artificial neural networks then need to learn several hundred training records containing a few hundred to a few thousand input nodes and possibly a few hundred to a few thousand output nodes. The optimization of the nets was discussed in a previous publication (Decker et al., July 1997). The current results were obtained with single hidden-layer

feedforward neural networks containing few hidden-layer nodes (sparse nets). About 3 hidden-layer nodes are required for each characteristic pattern (not each speckle pattern). Training time on the SGI O2 workstation was typically a few minutes for the entire training set.

The effectiveness of a computational model-to-test interface depends on the accuracy of the models. These models are discussed in the next section.

3. Models

3-1. Characteristic Fringe Pattern

The models of the characteristic fringe pattern have been defined in the references. The models are described briefly here, and some new features are discussed.

The quantity processed by the neural networks is the absolute value of a finite-element-resolution sampling of the expression

$$(\text{Speckle Pattern}) \times J_0(2\pi \mathbf{K}\cdot\boldsymbol{\delta}).$$

That expression would be generated experimentally by subtracting two 180-degree phase-shifted electronic holograms. The holograms are obtained from two adjacent frames or even and odd fields of the video. The work discussed in this paper was done entirely with frames. Evaluating the dot product of the sensitivity vector $\mathbf{K}$ and the displacement $\boldsymbol{\delta}$ requires the positions of the illumination source and the imaging lens, the geometry and sampling grid of the blade surface, and the vector-displacement field. The last two items are supplied with the finite element model described below. The finite elements and sampling grid generally are non-uniform; hence the models, the measurements and the display must handle non-uniform pixel sizes. The model has been supplied for the whole blade. Zooming on a small region of the blade requires interpolation on the generally non-uniform grid. Cubic interpolation is used for displacements and linear interpolation is used for grid coordinates, the components of the sensitivity vector and strains.

There are many potential complications in modeling the images and speckle patterns, including non-uniform illumination, aberrations, camera pixel saturation, distortion, quantization error, pixel response variations and speckle statistics. So far, the neural nets have proven to be quite robust in the presence of most of these effects, and the speckle effect has offered the major challenge. Speckle statistics, in principle, depend on the reference-to-object beam ratio and the surface microstructure of the blades (Goodman, 1975). For small beam ratios, a simple model is adequate. The intensity is distributed according to a negative exponential, and the phase is uniformly distributed in $(0, 2\pi)$. Random number generators select these quantities independently from pixel to pixel. In fact, provided that enough independent speckle patterns are included in the training set, variations in the speckle statistics do not seem to have a large effect on the performance of the nets (Decker et al., July 1997).

The macroscopic structure of the characteristic fringe pattern depends primarily on the finite element model described briefly in the next section.

3-2. Finite Element Model of Twisted Blades

A blade model with an airfoil section representative of a wide-chord fan was used to produce training sets for the neural network. The blade geometry is of constant cross-section and has a twist that varies linearly from 0 degrees at the root, to 30 degrees at the tip. Blade dimensions are chord, 8.72 cm. (3.433 in.); maximum thickness to chord ratio, 0.037; and span, 15.24 cm. (6.0 in.). A damaged and an undamaged blade were simulated with finite-element plate models.

Two finite element blade models were generated, one with a simulated crack and the other without. The crack is located at the root and extends from 87% to 100% of chord. The blades were structurally modeled as cantilevers by constraining the root nodes in all six degrees of freedom, except in the simulated crack region. The crack was simulated by releasing the constraints for all degrees of freedom at the nodes in its region. The finite element models have a 20x42 mesh of quadrilateral elements along the mid-thickness of the airfoil section (fig. 4). The blade material is 6061-T6 Aluminum with a Young's Modulus of 66.19 GPa (9.6×10^6 psi), a Poisson's Ratio of .33, and a Mass Density of 2712.832 kg/m^3 (2.536×10^{-4} lbs sec^2/in^4). Figure 4 shows both the blade mesh and the simulated crack location.

MSC/NASTRAN Solution 103 was used to solve for eight normal modes and frequencies, although only the first mode at about 199 Hz was used for this work. The eigenvectors were normalized with respect to the generalized mass. An output file of the eigenvalues, eigenvectors (displacements), and modal strains was then provided to train the neural network. A file of blade surface coordinates was also provided.

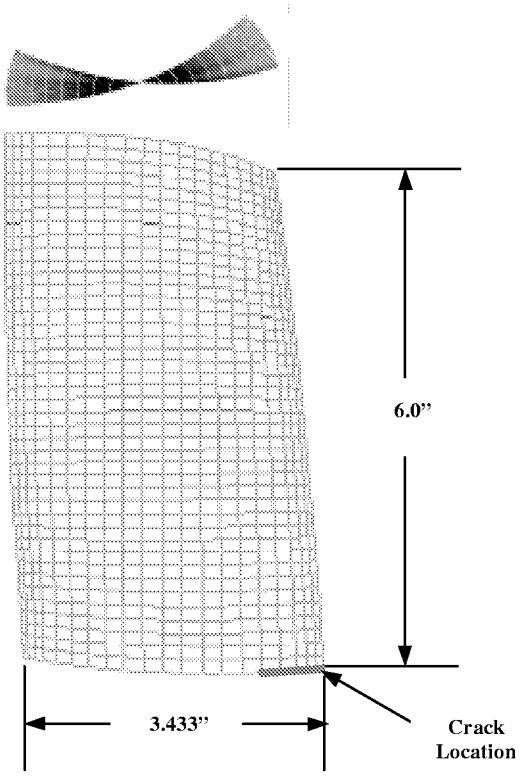

Fig. 4. Finite-element model of twisted blade showing crack location.

4. Performance of Neural Net for Detecting Blade Cracking for Measured and Model-Generated Characteristic Patterns

Three sample blades were manufactured according to the finite-element design discussed in sec. 3 in order to test the performance of the neural networks. The blades were painted flat white. The surface pattern from the brush strokes proved to be non-critical. Figure 5 shows that the blade and the blade mount are in fact machined from the same block of aluminum. The mount is held in a vice for subsequent tests. The vice torque is set to the same value for all tests. One of the blades, henceforth called blade 1, was intentionally cracked by inducing high-cycle fatigue failure on a shaker table vibrating at the frequency of the first mode (about 199 Hz). The crack developed in the region shown as an insert in fig. 1. The other two samples, henceforth-called blades 2 and 3, were undamaged.

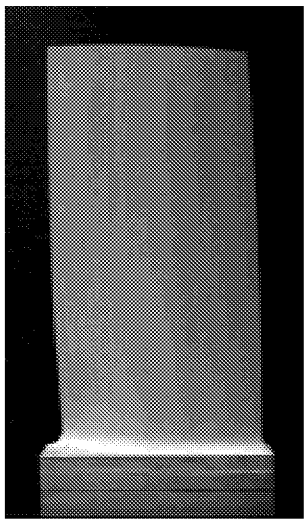

Fig. 5. Twisted blade and blade mount.

Initially, tests were performed on the whole-blade characteristic patterns of the first mode as shown in fig. 1. Maximum displacement amplitudes ranged from a small fraction of a micron to 50 microns. An interferometer was used to measure and set the vibration amplitudes. Hybrid training sets were used where the input characteristic patterns were recorded experimentally as discussed in sec. 2. The output vector contained the chord-wise second derivative of the model-generated field $\mathbf{K}\cdot\boldsymbol{\delta}$ as discussed in sec. 2. Second derivatives were evaluated numerically. Neural networks trained with the whole blade patterns generally could not distinguish the undamaged blades from the cracked blade. A change in approach was required.

The test procedure was changed after noting that the resonant frequency of the cracked blade decreased from 199 Hz to 195 Hz as the vibration amplitude was increased. The frequency change first appeared when the amplitude of vibration was increased above 50 microns. However, the contrast of the whole-blade Bessel characteristic pattern became too small when the vibration amplitude was increased above 50 microns. Hence, the decision was to zoom onto the insert region shown in fig. 1 for subsequent measurements. The amplitude of vibration remained small and the pattern contrast remained high in the zoomed region. The neural networks began to distinguish the cracked blade from the undamaged blade at tip vibration amplitude of 50 microns. The settings for the remaining discussions were 273 microns. It should be noted that the tip deflections were inferred at amplitudes larger than 50 microns. The amplitude was measured using the interferometer near the insert region shown in fig. 1, and the finite element model was used to estimate the tip deflection

The measured region in the insert in fig. 1 extended span-wise from the mount and chord-wise to the right edge of the blade. The width of the region equaled 0.5 in. (1.27 cm) and the height equaled 0.438 in. (1.111 cm). The performances of two neural-net architectures were tested. The composition of the training records was discussed in sec. 2. The inputs consisted of experimentally measured patterns from blades 1 and 2. A 903 node input vector was used. Blade 1 was also used to generate zero-amplitude training records. One hundred training records per blade or condition were recorded in accordance with the ten-percent rule mentioned in sec. 2. The two net architectures differed only in the output vectors. The chord-wise second derivatives of the model-generated field $\mathbf{K}\cdot\boldsymbol{\delta}$ were used in the output vector for one architecture. A simple color-coded output was used for the other architecture. In terms of normalized outputs, the code was (0.8, 0.2, 0.2) for green, (0.2, 0.8, 0.2) for yellow and (0.2, 0.2, 0.8) for red. For display purposes at 30 frames per second, the model-generated output was displayed as a density plot. The color code, on the other hand, was used to set the color of a 30-frame-per-second display of the characteristic pattern at CCD or finite-element resolution. The color was green for undamaged blades and red for cracked blades. The yellow color was used to indicate either the zero amplitude (speckle noise only) condition or a no-decision condition. The maximum component of the color vector was required to be 0.8 ± 0.05, otherwise a no-decision was declared. Both neural-net architectures contained 6 hidden-layer nodes.

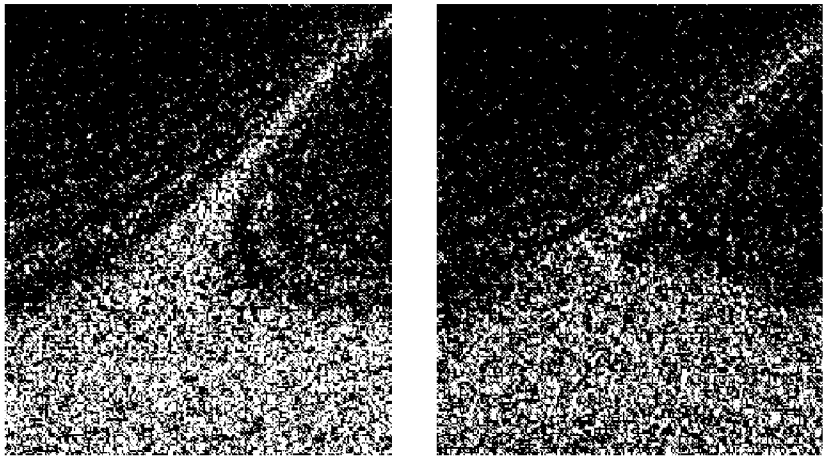

Fig. 6. Measured-region experimental characteristic patterns: (a) for undamaged blade, (b) for cracked blade.

Figure 6 shows the measured region experimental characteristic patterns for the undamaged and cracked blades. Figure 7 shows model generated characteristic patterns for an undamaged blade at two different finite element resolutions.

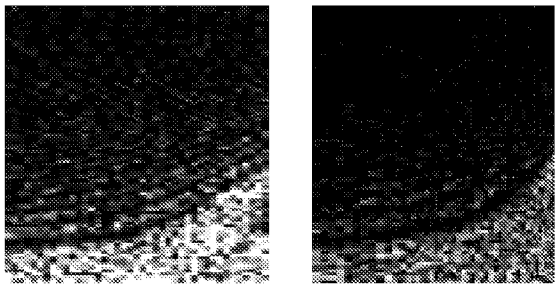

41 X 85 51 X 101

Fig. 7. Model-generated characteristic patterns for an undamaged blade at two finite element resolutions.

Both neural-net architectures performed well when presented with blade 1, 2 or 3 experimental characteristic patterns at tip deflections of 273 microns. But neither neural network performed well when presented with the model-generated characteristic patterns.

5. Discussion of Performance of Neural Nets

The experimentally trained neural networks did not respond correctly to the model generated data, and the reason is clear from comparing fig. 6 with fig. 7. The finite-element-model and experimental patterns are not similar in the measured region.

In fact, the twisted blade results are disappointing in two ways when compared with previous work with cantilever plates. First, twisted blade damage was not detectable from the entire blade characteristic pattern; whereas damage was detectable from an entire cantilever-plate pattern at low excitation amplitudes. The expectation, following the cantilever-plate work, was that the entire-blade characteristic pattern would serve as a neural-net-processed gauge of blade damage. Second, the finite element models used for design did not reproduce the correct twisted blade patterns. The models did produce the correct cantilever patterns. Figure 8 (Decker et at., July 1997) compares model generated and measured characteristic patterns for the first chord-wise mode of a cantilever. The model-generated and experimental patterns look quite similar, and a neural network can be trained to distinguish damaged from undamaged blades using the entire-cantilever characteristic pattern.

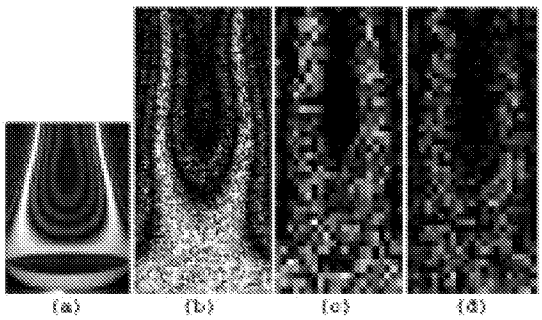

Fig. 8. First chord-wise mode: (a) from a silver halide hologram of a vibrating blade, (b) from electronic holograms of a vibrating cantilever, (c) from a finite-element-resolution model of a cantilever plate, (d) from electronic holograms at finite-element resolution.

6. Concluding Remarks

Artificial neural networks could not be used to create a practical model-to-experiment interface when trained with a design-grade finite element model. The model could not create the detail that electronic holography can measure. There are fracture mechanics models that generate better structural detail, but one of our objectives was to create a good design-to-test interface. The workstation-resident design-grade models were not adequate for this purpose.

The nets trained with experimental inputs were able to detect structural damage and to display the damage using model- generated or damage-flag outputs. Hence, the nets are good tools for testing whether a model is adequate: train the nets experimentally and then use the model to generate inputs to be evaluated by the trained nets.

Experimentally trained nets can also be used to create a record of an undamaged part to be used for later inspections.

A question relevant to this conference concerns the potential usefulness (not merely the possibility) of using model trained neural networks for flow applications. For example, are model trained neural networks useful for performing tomography? The best judgement at this time is that the neural-net application can be useful for flow conditions that remain essentially the same year after year. An example would be a wind tunnel operated essentially the same way for years. Then the neural net can be trained with much effort to respond to the important details and to ignore the irrelevancies, just as a net was trained to ignore the laser speckle effect.

References

Decker, A. J., "Neural networks for calibration tomography", *Optical Diagnostics in Fluid and Thermal Flow, Proc. SPIE,* **vol. 2005,** pp. 562-569, 1993.

Decker, A. J., Fite, E. B., Mehmed, O. and Thorp, S. A., "Processing speckle patterns with model trained neural networks", *Optical Technology in Fluid, Thermal, and Combustion Flow III, Proc. SPIE,* **vol. 3172,** pp. 285-293, July 1997.

Decker, A. J., Fite, E. B., Mehmed, O. and Thorp, S. A., "Vibrational Analysis of Engine Components Using Neural-Net Processing and Electronic Holography", *Advanced Non-Intrusive Instrumentation for Propulsion Engines, AGARD-CP-598,* pp. 33-1—33-6, May 1998.

Vest, C. M., *Holographic Interferometry,* pp. 177-217, Wiley, New York, 1979.

Goodman, J. W., "Statistical properties of laser speckle patterns", *Laser Speckle and Related Phenomena,* Dainty, J. C., ed., pp. 29-35, Springer-Verlag, Berlin, 1975.

REPORT DOCUMENTATION PAGE

Form Approved
OMB No. 0704-0188

1. AGENCY USE ONLY (*Leave blank*)	2. REPORT DATE	3. REPORT TYPE AND DATES COVERED
	November 1998	Technical Memorandum

4. TITLE AND SUBTITLE

Comparison of Computational–Model and Experimental–Example Trained Neural Networks for Processing Speckled Fringe Patterns

5. FUNDING NUMBERS

WU–519–30–53–00

6. AUTHOR(S)

A.J. Decker, E.B. Fite, S.A. Thorp, and O. Mehmed

7. PERFORMING ORGANIZATION NAME(S) AND ADDRESS(ES)

National Aeronautics and Space Administration
Lewis Research Center
Cleveland, Ohio 44135–3191

8. PERFORMING ORGANIZATION REPORT NUMBER

E–11413

9. SPONSORING/MONITORING AGENCY NAME(S) AND ADDRESS(ES)

National Aeronautics and Space Administration
Washington, DC 20546–0001

10. SPONSORING/MONITORING AGENCY REPORT NUMBER

NASA TM—1998-208814

11. SUPPLEMENTARY NOTES

Prepared for the International Conference on Optical Technology and Image Processing in Fluid, Thermal and Combustion Flow, cosponsored by the Visualization Society of Japan and SPIE - The International Society of Optical Engineering, Yokohama, Japan, December 7–9, 1998. A.J. Decker, E.B. Fite, S.A. Thorp, and O. Mehmed, NASA Lewis Research Center. Responsible person, A.J. Decker, organization code 5520, (216) 433-3639.

12a. DISTRIBUTION/AVAILABILITY STATEMENT

Unclassified - Unlimited
Subject Categories: 35, 39, and 59 Distribution: Nonstandard

This publication is available from the NASA Center for AeroSpace Information, (301) 621–0390.

12b. DISTRIBUTION CODE

13. ABSTRACT ***(Maximum 200 words)***

The responses of artificial neural networks to experimental and model-generated inputs are compared for detection of damage in twisted fan blades using electronic holography. The training-set inputs, for this work, are experimentally generated characteristic patterns of the vibrating blades. The outputs are damage-flag indicators or second derivatives of the sensitivity-vector–projected displacement vectors from a finite element model. Artificial neural networks have been trained in the past with computational-model-generated training sets. This approach avoids the difficult inverse calculations traditionally used to compare interference fringes with the models. But the high modeling standards are hard to achieve, even with fan-blade finite-element models.

14. SUBJECT TERMS

Neural networks; Interferometry, Electronic holography; Image processing; Speckle metrology

15. NUMBER OF PAGES

14

16. PRICE CODE

A03

17. SECURITY CLASSIFICATION OF REPORT	18. SECURITY CLASSIFICATION OF THIS PAGE	19. SECURITY CLASSIFICATION OF ABSTRACT	20. LIMITATION OF ABSTRACT
Unclassified	Unclassified	Unclassified	